# SITE EFFECTS IN A TWO-DIMENSIONAL VALLEY STRUCTURE: COMPARISON BETWEEN OBSERVATIONS AND NUMERICAL SIMULATIONS

D. Jongmans[1] and M. Campillo[2]

## ABSTRACT

A temporary network of five 3 component seismometers was set up during one month in a small valley of the French Alps. The records of 15 earthquakes, whose magnitude is ranging from 1.0 to 3.6, were analyzed. The geological structure, which was poorly known, has been investigated by different seismic methods. From the survey, both the geometry of the layers and their dynamic characteristics ($V_S$, $V_P$, $Q_S$ an $Q_P$) were derived.

On this basis, the 2D valley response has been computed by a boundary integral equation method in the SH case. The comparison between experimental and theoretical data is generally good, at least for frequencies lower than 10 Hz. In other cases of input, the data exhibit a great variability between different groups of similar earthquakes and more sophisticated simulations (2D P-SV, 3D) should be used.

## INTRODUCTION

Local soil conditions can lead to significant variations in ground motion generated by earthquakes. These amplification effects have been studied numerically and experimentally by numerous authors (for a review, see Aki [1]). However, few comparisons have been made between observations and theoretical results for well-known 2D structures.

In this paper, we present a global study of the response of a small valley located in a moderate seismicity area (Alps-France). The report is divided into three main parts. The first one is devoted to the investigation of the geological structure of the valley, which was previously unknown. Various geophysical methods, including refraction tests, reflection survey and surface wave analysis, were used to infer both the structure and the dynamic characteristics ($V_P$, $V_S$, $Q_P$ and $Q_S$) of the layers.

In the second part, we investigate the earthquake ground motions measured during one month by a temporary array of five 3 component seismometers.

[1] LG I.H., Université de Liège, Bat B19, 4000 Liège, Belgium
2 LG I.T., Université Joseph Fourier, BP 53X, 38041 Grenoble, France

Finally, we present a comparison of the experimental response of the valley with the prediction of 1D and 2D models derived from seismic surveys.

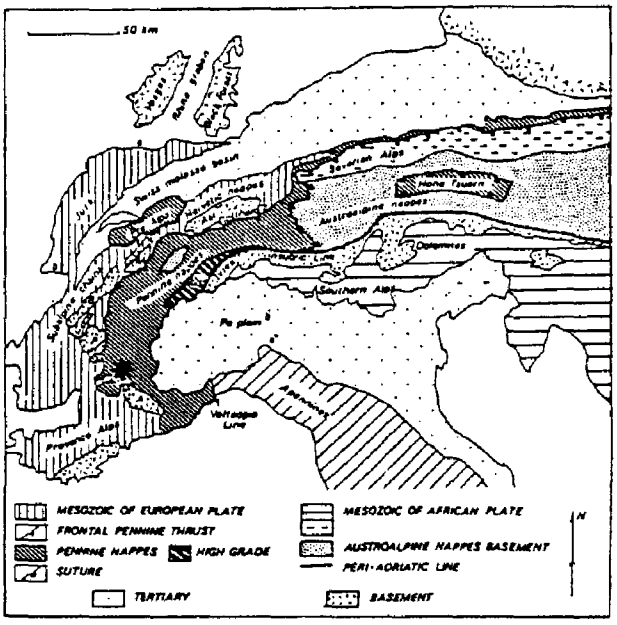


FIGURE 1. Geological map of the Alps (after Coward and Dietrich, 1990). The Ubaye valley is indicated by a star.

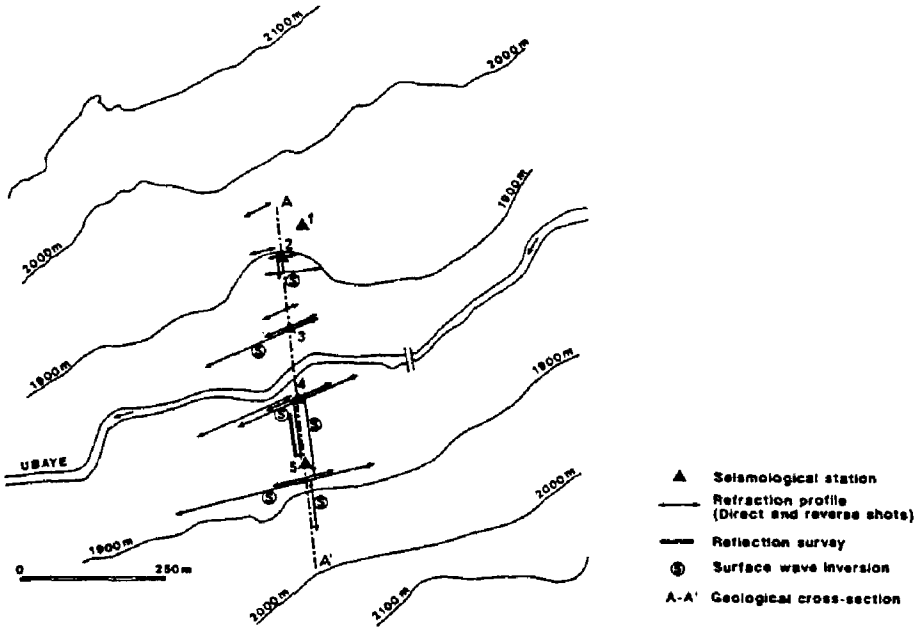


FIGURE 2. Map view of the experiment site with the locations of the seismic surveys

## GEOLOGICAL SETTING AND SEISMIC SURVEY

The site of the experiment is located in the French Alps close to the Italian border (see Fig.1). This zone belongs to the Briançonnais arc which is an internal unit of the western Alps. It consists of a siliceous basement (Permo-Carboniferous age) overlain by a calcareous cover (Mesozoïc and Eocen).

The location of the experiment site was chosen in the Ubaye valley, near the village of Maljasset, for three main reasons: the level of seismicity of the area, the moderate dimensions (5OO meters wide) of the structure and the shape of the valley which may be considered as two-dimensional (Fig.2).

The bedrock consists of Cretaceous limestone which outcrops on the slopes. The valley filling is a mixture of moraine, alluvium and alluvial fans.

**Refraction survey**

The geophysical investigation has included 17 refraction profiles (P wave) of 24 to 360 meters long. The sources used were a hammer for the shortest profiles and explosives for long distances. Several S-wave refraction profiles were additionally performed, with a maximum distance source-receiver of 180 meters. The horizontal impact of a hammer onto one side of a loaded plank was used as a shear wave source. The location of the different seismic profiles is shown in Figure 2. An example of a time-distance curve (P-wave) for a long profile is presented in Fig. 3.

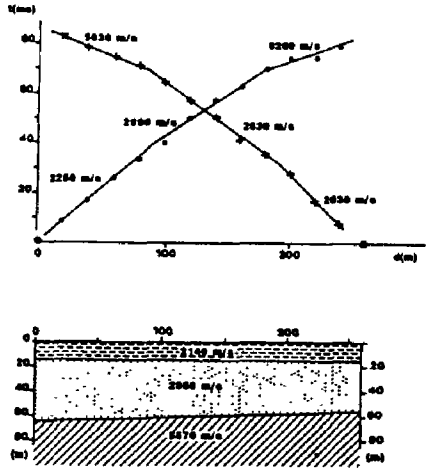

FIGURE 3. Top: direct and reverse traveltime-distance graphs for a shot carried out in the Ubaye valley - Bottom: interpretation of the structure from the refraction data, showing the different layers.

**Surface wave analysis**

During the refraction survey, the record duration was increased in order to get the surface waves. Field seismograms measured by vertical 4.5 Hz geophones, between 120 m to 240 m from the source, are shown in Fig.4.

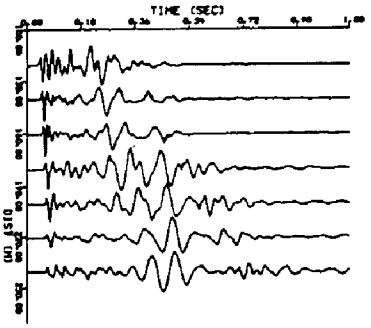

FIGURE 4. Field seismograms (vertical component) measured in the Ubaye valley.

The processing of surface waves, which clearly dominate the signal, has allowed us to derive S-wave velocity profiles. Both phase and group velocity dispersion curves are computed, using the software developed by Herrmann [2]. These data, whith frequencies ranging from 6 to 15 Hz, are presented in Fig.5 .They are used in an iterative inversion process in order to infer the distribution of S-wave velocity at depth.

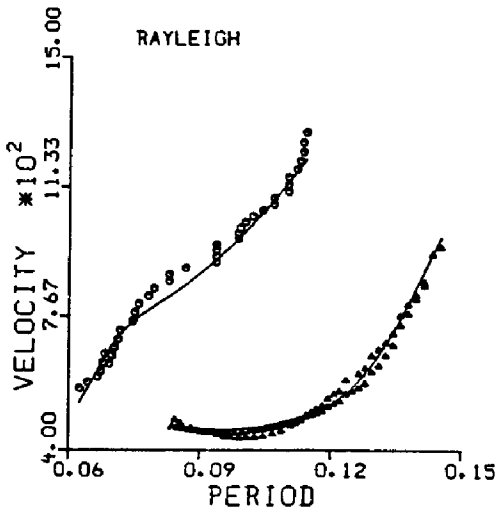


FIGURE 5. Theoretical (lines) and experimental (triangles : group velocity - hexagons : phase velocity) dispersion curves.

The theoretical dispersion curves are also plotted on Fig.5, whereas the final model is shown in Fig.6. It is compared with the vertical S-wave profile deduced from refraction surveys at the same site. A low velocity layer appears at about 20 meters depth. The results are however consistent with the refraction data. The right side of Fig.6 gives the resolving kernels at each depth.

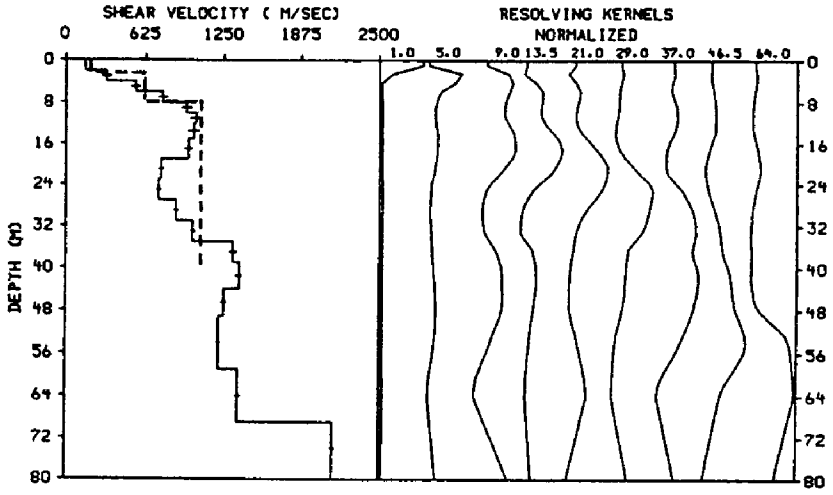


FIGURE 6. Left: S-wave profile compared to the refraction results (dashed line) - Right: Resolving kernels at 1, 5, 9, and 64 meters.

Another example, showing the application of Love waves at short distance (10 to 20 meters) from the source, is presented in Figs. 7 and 8.

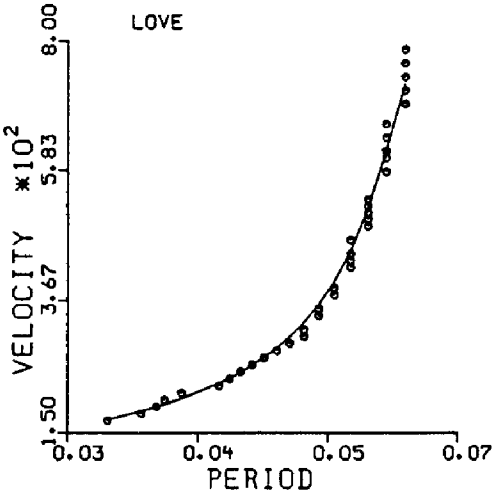


FIGURE 7. Theoretical (line) and experimental (hexagons) dispersion curves of the phase velocity (Love waves). Note the period range, lower than in the case of Fig.5.

In this case, the frequency range is between 15 and 30 Hz. The final model, obtained from the

iterative inversion process (Fig.8), shows the presence of low velocity layers at shallow depth (0-3 m). The resolution is good for layers whose depth is less than 3 meters. The two cases presented above illustrate the interest to process surface waves with different frequency contents for the definition of S-wave velocity profile at the same site.

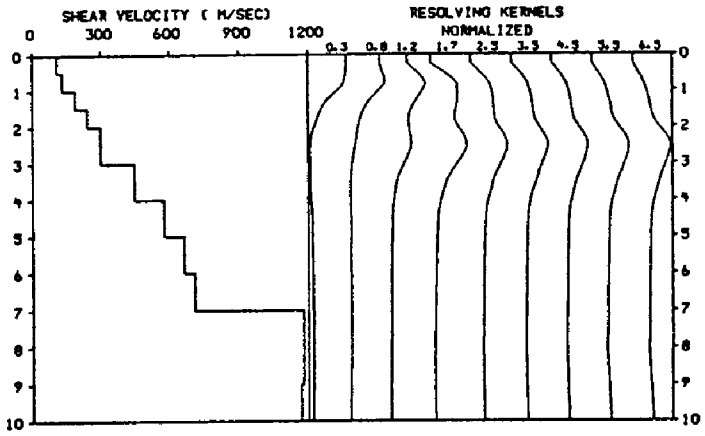


FIGURE 8. Left: S-wave profile as a function of depth. - Right: Resolving kernels.

**Reflection profile**

A high resolution reflection profile was also carried out in order to map the limestone bedrock in the central part of the valley.

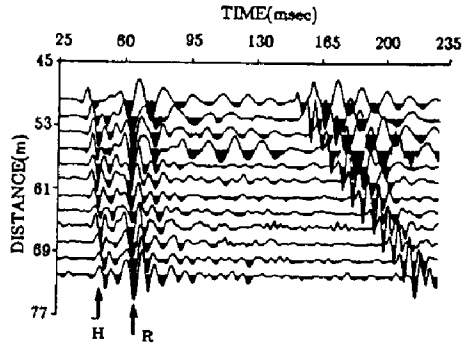


FIGURE 9. Typical field seismograms of a reflection test. Head waves and reflection from the bedrock are marked with "H" and "R".

The data were collected using a gun as a source and twelve 50 Hz geophones. From walkaway tests, an offset of 50 meters and a geophone interval of 2 meters were chosen.In order to reduce the effects of ground roll, an analog low-cut filter of 100 Hz was applied to the data.

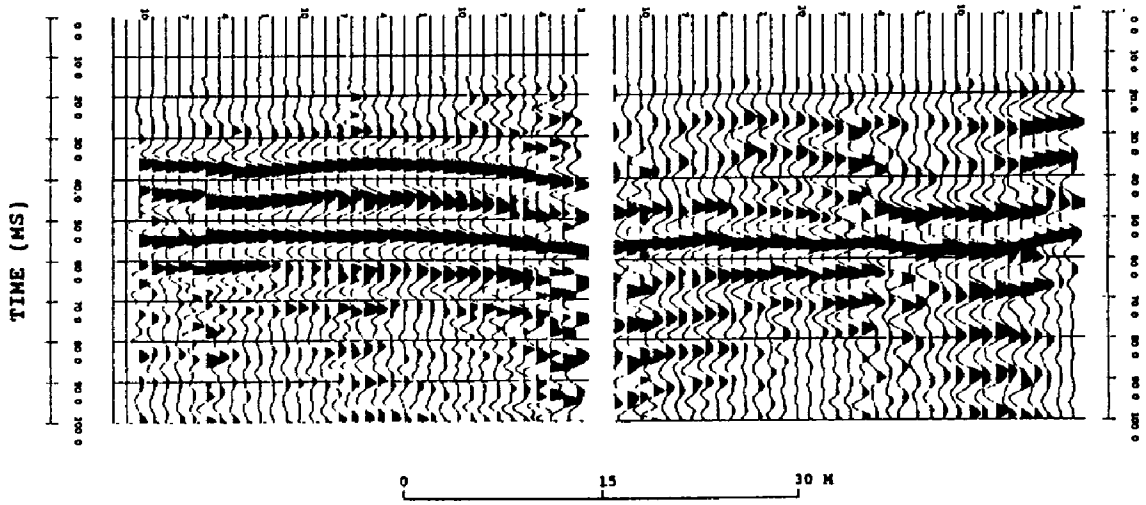


FIGURE 10. Final seismic section.

Fig.9 shows typical field seismograms, with head waves and the reflection from the berock at about 60 ms. As a result of the data processing, the final seismic section is presented in Fig.10. The bedrock reflector, which is the only regular event present on all the section, appears at about 55 ms.

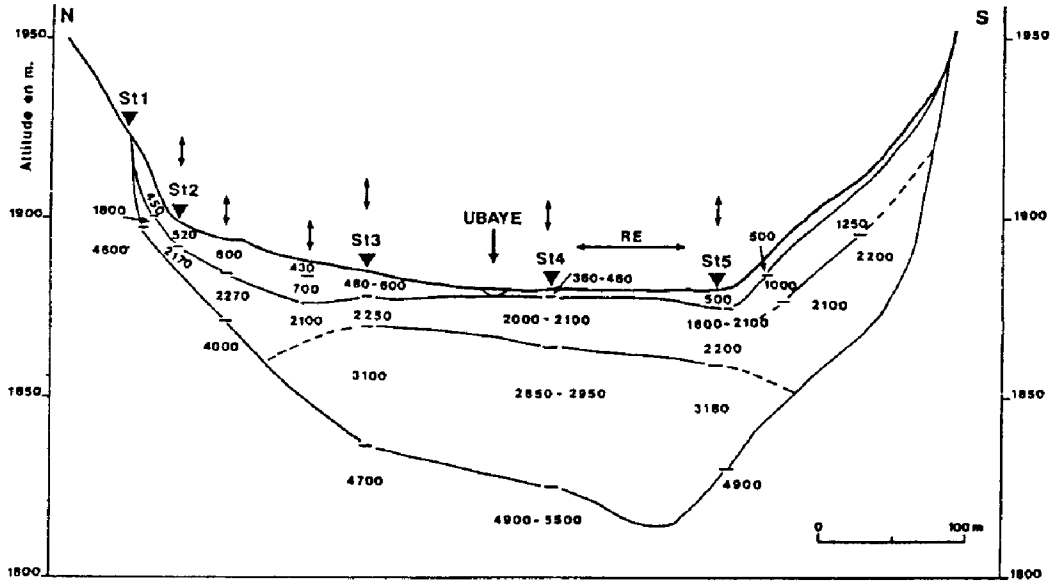


FIGURE 11. Cross section along the profile AA' (Fig.2) with the P-wave velocity values in the different layers

**Geological structure**

The NNW-SSE cross section, derived from geophysical prospecting is presented in Figs. 11 and 12, with P- and S-wave velocities respectively.

The results obtained indicate that the underground structure consists of four layers. The bedrock is composed of sound limestone with P wave velocity varying from 4500 to 5500 m/sec (Vs =2100-2400 m/s).

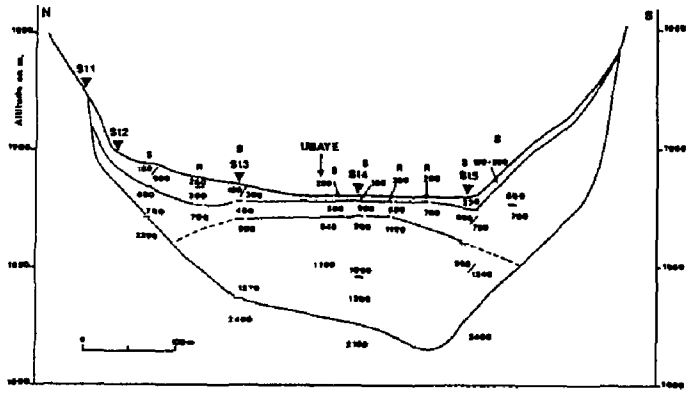


FIGURE 12. Cross section along the profile AA' (Fig.2) with the S-wave velocity values in the different layers.

The top of the substratum is mapped at a maximum depth of 65 m in the central part of the valley. It is overlaid by three different units (from top to bottom) :

- a soft surficial layer (formation 1) with P-wave velocities ranging from 360 to 600 m/s. It is made up of recent alluvium from the Ubaye River and of colluvium from the relatively steep shoulders of the valley. The mean S-wave velocity is low (Vs = 250 m/s).

- formation 2 is characterized by S-wave velocity values ranging from 500 to 700 m/s, while P-wave velocities are generally between 2000 and 2200 m/s. It may correspond to a mixture of alluvium and alluvial fan. This unit exhibits great variations of thickness along the profile.

- formation 3, overlying the bedrock in the central part of the valley, presents relatively high velocities (Vs 1100 m/s and $V_p$ 3000 m/s) which may correspond to overconsolidated moraine or weathered bedrock

The simplified configuration used later for numerical simulations is shown in Fig.13.

**Quality factor determination**

Besides the geometry of the interfaces and the different wave velocities, we need another important parameter to compute the valley response : the shear wave quality factor Qs. The problem we address is to determine soil Q values from seismic survey data.

Among the various methods proposed to compute Q, the following ones were previously tested by one of us [3] on synthetic seismograms: the rise time method, the surface wave attenuation study (SWAS) and the spectral ratio method. From this work, it appeared that the first two techniques are able to deduce correct Q values in a horizontal layered medium. On the other hand, the spectral ratio method, applied to refraction data, was found less reliable, owing to the difficulty to obtain a signal part free from interference. For this reason, this approach was not used and only the two others methods are discussed further.

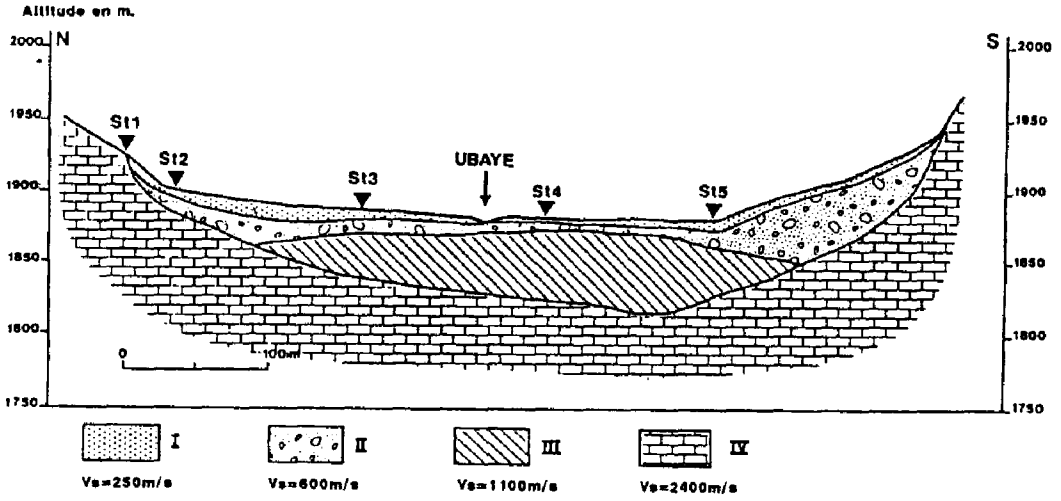


FIGURE 13. Idealized cross section showing subsoil conditions along the trace AA' (Fig.2).

However, attenuation measurements remain a crucial problem, mainly because of the question of the frequency dependence of Q. A lot of literature is devoted to this difficult subject (see, for a review, Johnston and Toksöz [4]). In geophysical prospecting and earthquake engineering, the usual assumption, based on a large amount of data, is that Q is independent of frequency. However, some experiments, both in the field (Meissner and Theilen [5]) and in the laboratory (Johnston and Toksöz [4]), show clear variations of Q with the frequency. One explanation could be the occurrence of scattering on heterogeneities at different scales. Our aim is, however, to determine realistic values of Q for earthquake simulations and attenuation measurements will be carried out in different frequency ranges.

**The rise time method**

The rise time method is based on the broadening of the first pulse resulting from the attenuation of the high-frequency components. The rise time $\tau$ was defined by Gladwin and Stacey [6] as the ratio of the maximum peak amplitude to the maximum slope of the first quarter-cycle of the pulse. From their experiments, they proposed the following relationship:

where $\tau$ and $\tau_0$ are the rise times at the measurement point and at the source, t is the traveltime and C is a fixed constant.

As pointed out by Blair and Spathis [7], the factor C is source dependent and has to be estimated for each data set. The way to overcome this difficulty is to simulate the wave propagation in an attenuating medium (with a constant Q value) and to compare the results to the data.

This method has been applied to the S-wave refraction data recorded in the Ubaye valley. Fig. 14 shows an example of field seismograms and the corresponding $\tau$-t diagram characterizing formation 3. The frequency range of the signal is between 25 and 60 Hz. Beyond a distance of 1.2 wavelength, the relation between $\tau$ and t is almost linear and the rise time method leads to a Qs value of 5.4 . At close distance from the source, the pulse shape is mainly controled by the near-field terms and the onset of surface waves (Jongmans,[8]).

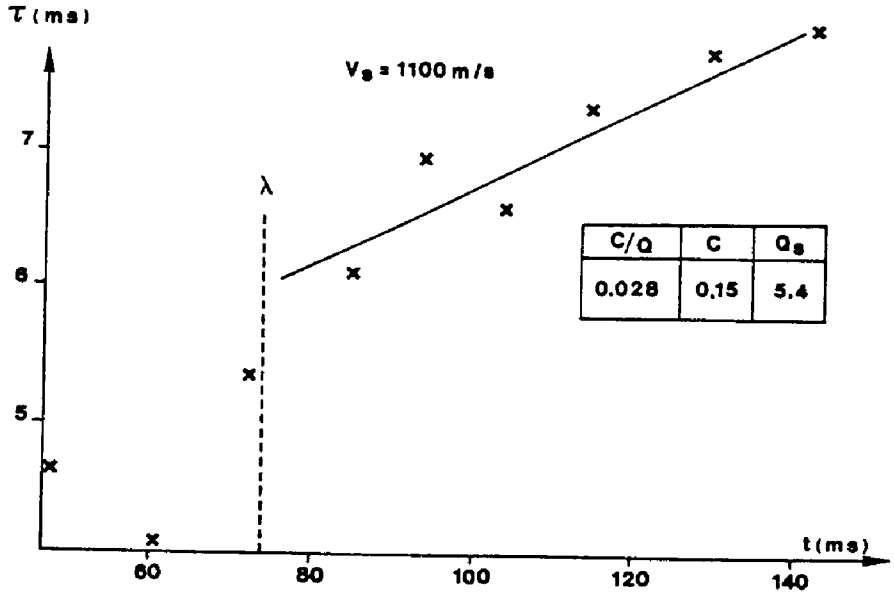


FIGURE 14. Rise time as a function of the traveltime.

**Surface wave attenuation study (SWAS)**

The SWAS method consists in computing the frequency dependent attenuation factor of the surface wave amplitude (Herrmann,[9]). These data are then inverted in order to obtain a vertical $Q_S$ profile.

From the field seismograms, plotted on figure 4, we have computed the attenuation curve presented at the top of Fig.15. The FIGURE 15. Left: Experimental and theoretical attenuation curves for surface waves.- Right: $1/Q_S$profile and resolving kernels.

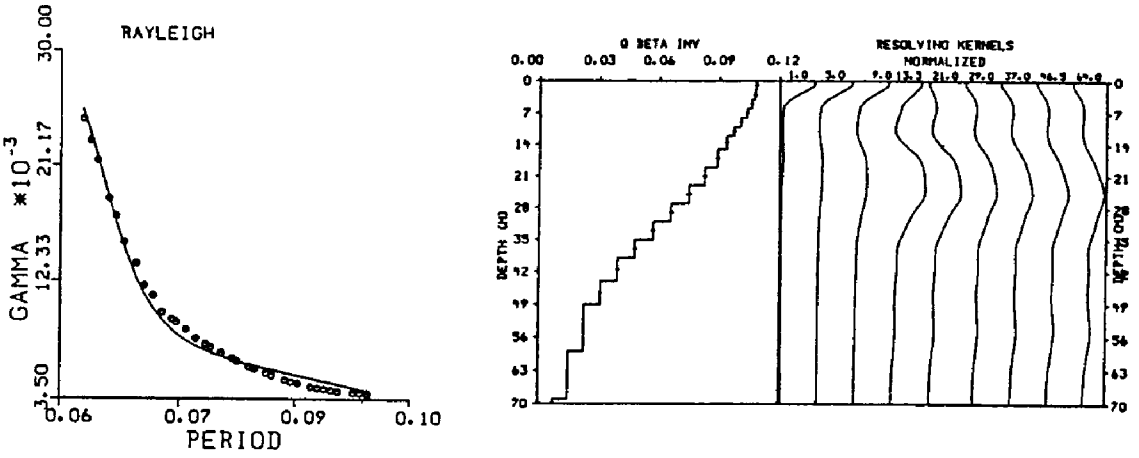


Frequency range of the signal varies between 9 and 16 Hz. The inversion of the attenuation data leads to the $1/Q_S$ profile and the resolving kernels shown at the bottom of Fig.15.

**$Q_S$ values**

All the results of Qs determinations are presented in Table 1. In a general way, Qs values obtained at high frequency (25-60 Hz) with the rise time method are about 5 to 6 in formations 2 and 3. They are systematically lower than those inferred from Rayleigh waves in a lower frequency range (9-16 Hz). These results, also observed on other sites by Jongmans [3], may indicate a frequency dependence of Q in surficial materials.

As we will see later, higher $Q_S$ values (10 to 20) are far more consistent with the experimental valley response.

TABLE 1. $Q_s$ and $Q_P$ values inferred from in-situ tests.

| Unit | Method | Qp | Qs | Frequency (Hz) P | S |
|---|---|---|---|---|---|
| 2 | Rise time | 5.5-7.5 | 5-6 | 50-90 | 40 |
| | Surface wave | — | 10 | — | 9-16 |
| 3 | Rise time | 11 | 5-6 | 60-100 | 30-50 |
| | Surface wave | — | 20 | — | 9-16 |

## SEIMOLOGICAL DATA ACQUISITION

During one month (May 1989), a temporary network of 5 seismological stations was installed in the site of Maljasset (see Fig. 2 for their location). We used identical digital stations composed of 3 component seismometers with natural frequency of 2 Hz.

The NS component approximately corresponds to the direction of the profile whereas the EW component refers to the direction along the valley axis. A reference station was positioned on a limestone outcrop. The other stations were set up at equal interval across the valley.

In order to study the experimental site response, we selected the events recorded by at least 3 stations. The locations of the 15 earthquakes used in the following analysis are shown in Fig. 16 while their main characteristics are given in Table 2. We organized this set of earthquakes into 3 groups with respect to their locations

In order to verify that this choice is sound, the spectra of the horizontal motions (S waves) at the hard rock station are compared for the different events and the analogy of the shape of the spectra is checked.

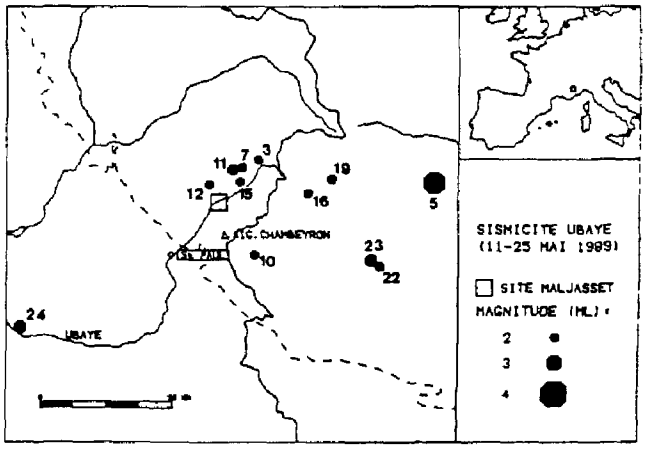


FIGURE 16. Sketch map of the area with the locations of earthquakes.

The earthquakes are subdivided as follows:

- group 1 : events 7, 10, 11, 12 and 13
- group 2 : events 15, 16 and 19
- group 3 : events 22, 23 and 24.

The event 05 is different from the others both by its magnitude (3.6) and its location. Group 1 consists of local shallow earthquakes that occurred in the North of the site in the direction of the alignment of our stations. The epicentral distances are less than 10 km. Groups 2 and 3 correspond to earthquakes located at distances larger than 15 km and 25 km, respectively.

TABLE 2. List of the earthquakes with their main characteristics.

| number | date | hour | $M_L$ | $t_s-t_p$ (sec.) | epicentral distance (km) | depth (km) |
|---|---|---|---|---|---|---|
| 3 | 11-05 | 13h40 | 2.2 | 1.12 | 9.6 ± 2 | 4 ± 3 |
| 5 | 12-05 | 11h27 | 3.6 | 3.79 | 34.3 ± 2 | 9 ± 4 |
| 7 | 17-05 | 03h09 | 2.3 | 0.46 | 6.9 ± 2 | 0 ± 2 |
| 10 | 17-05 | 06h04 | 0.5 | 0.55 | 10 ± 26 | 0 ± 8 |
| 11 | 17-05 | 07h59 | 2.5 | 0.54 | 6 ± 3 | 3 ± 2 |
| 12 | 17-05 | 08h12 | 1.8 | 0.54 | 3.2 ± 1 | 2.8 ± 0.5 |
| 13 | 17-05 | 08h14 | < 2 | 0.52 | — | — |
| 15 | 18-05 | 12h16 | < 2 | 2.30 | 4.5 ± 3 | 16 ± 1 |
| 16 | 18-05 | 13h03 | 1.9 | 2.18 | 14.4 ± 2 | 9 ± 1 |
| 19 | 22-05 | 20h05 | 2.3 | 2.00 | 18.5 ± 2 | 7 ± 2 |
| 20 | 22-05 | 20h46 | < 2 | 0.53 | — | — |
| 21 | 25-05 | 13h32 | < 2 | 0.55 | — | — |
| 22 | 25-05 | 13h51 | 2.4 | 3.30 | 27.3 ± 1 | 2 ± 2 |
| 23 | 25-05 | 18h58 | 2.7 | 3.24 | 26.1 ± 1 | 7 ± 2 |
| 24 | 25-05 | 22h00 | 2.7 | 3.50 | 36.5 ± 2 | 3 ± 3 |

## EXPERIMENTAL SITE RESPONSE

An example of seismograms recorded at the five stations are

presented in Fig.17 .The signal duration is 25 seconds. The records, plotted with the same scale, illustrate the amplification of the ground motion in the valley with respect to the hardrock site. The amplification appears on all the components, except on the EW horizontal component which was inoperative.

In order to quantify this amplification effect, spectral ratios were computed by dividing each spectrum obtained in the valley by the corresponding spectrum observed at the reference station.

Fig.18 shows the spectral ratios (Group 1) computed for the EW horizontal components as well as the mean spectral ratio drawn with dashed lines.

At each station the ratios exhibit some very similar features in most cases. The existence of spectral bands of amplification centered on the same values of frequency is characteristic of the response of the soft deposits.

We have just shown the relative stability of the spectral ratios for earthquakes of a given group but this property no longer exists when comparing records for events from different groups. This is illustrated with Fig.19 which shows the mean values of the spectral ratio computed for each group of earthquakes. We have plotted separately the curves corresponding to the earthquake 05 which has a magnitude and an epicentral distance different from the other events.

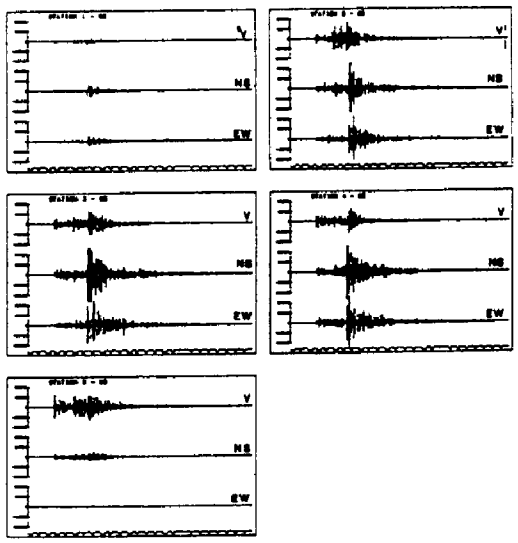

FIGURE 17. Seismograms (25 sec.) recorded during earthquake 05 at the 5 stations on 3 components.

In some cases we have also computed the spectral ratio for the seismic noise. The clear difference between the results obtained from earthquakes and from noise is probably due to the part played by the river. The spectral ratios computed for the earthquake roups show in most cases some differences that prevent a common response of the sites being identified.

From the examination of these figures we can draw the following conclusions:

- the spectral amplifications vary from one station to another both in terms of maximum value and of shape of the response curve.

- the spectral ratios seem to be also dependent on the group of earthquakes considered.

In order to further understand the amplification effects and their variability, we have compared these observations with theoretical predictions made using under simple assumptions.

## NUMERICAL SIMULATION

To compute the response of a two dimensional structure given by the results of the prospection (Fig. 13), we used a boundary integral equation method in a formulation described by Bouchon et al. [10].

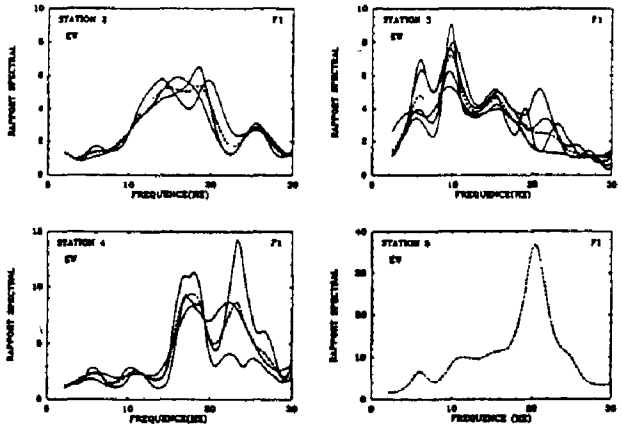

FIGURE 18. Spectral ratios for the events of Group 1 (EW component). The mean value is plotted as a dashed line.

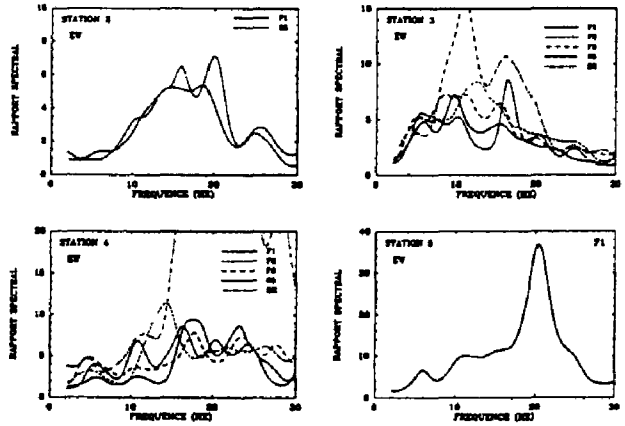

FIGURE 19. Comparison between the mean spectral ratios computed for the different groups of earthquakes. The curves corresponding to Group 1 to 3 are labelled F1 to F3. The dashed line (BR) is the mean ratio obtained from the seismic noise.

This method enables us to consider steep interfaces and high frequency waves. In the present application, we restricted the computation to the case of vertically incident SH waves. We considered frequencies between 0 and 25 Hz. The model was simplified in order to give a local analytic representation of the

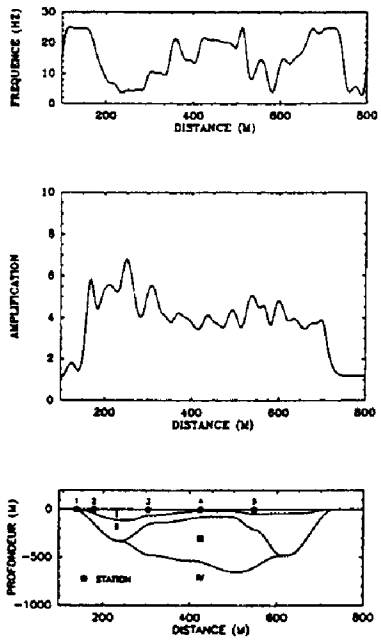


FIGURE 20. Bottom: 2D model used in the computations. - Middle: Maximum amplification.- Top: frequency corresponding to this maximum.

TABLE 3. Dynamic characteristics of the formations used for 2D modeling.

| formation n° | description | $V_s$(m/s) | $Q_s$ | $\rho$ |
|---|---|---|---|---|
| 1 | Surficial layers (alluvium, colluvium) | 250 | 10 | 1.8 |
| 2 | Alluvial deposits | 600 | 10 | 1.9 |
| 3 | Moraines, weathered bedrock | 1100 | 20 | 2.0 |
| 4 | Limestone | 2400 | 200 | 2.6 |

interfaces in terms of cosines. It is presented in Fig.20 together with the maximum values of amplification and the corresponding frequencies. The parameters of the medium used are given in Table 3. The quality factors are those inferred from surface wave analysis.

The results obtained indicate the existence of low frequency amplification above deep soft deposits. The maximum values of amplification are less than 7. The wave propagation in the valley can be seen in Fig. 21 which illustrates a section of synthetics seismograms computed across the structure. These synthetics correspond to an incident Ricker wavelet whose central frequency is 10 Hz. It is not possible to identify waves that propagate from one edge of the valley to the other. Thus we cannot expect to observe a lateral resonance of the structure. On the contrary, in each of the two zones where the layers 1 and 2 are thick, we can see travelling waves that contribute to increase the duration of the signal and, therefore, that are the cause of the spectral amplification shown in Fig.20.

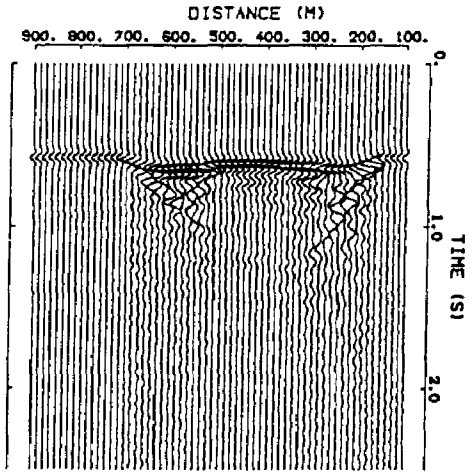


FIGURE 21. Synthetic seismograms computed for the model shown in Fig.20. The source time function is a Ricker wavelet of central frequency 10 Hz.

**Comparison between observed and predicted amplifications**

The results are summarized in Fig.22 which presents the spectral ratios computed from the EW components of earthquake records of group I and the theoretical spectral amplifications for the 1D and 2D computations. The most striking effect of considering a 2D model in place of a 1D one is visible for the case of Station 2. As this is observed, the two-dimensional modeling predicts a broad-band amplification of the motion while a flat layered structure would result in a peaked spectrum. For station 3, our results are almost similar whatever model is considered. The prediction slightly underestimates the amplification beneath the station but gives an acceptable description of the location of the peaks of amplification. For Station 4 the models and the

observations are in good agreement for frequencies smaller than 10 Hz. At high frequencies, the large discrepancy is probably explained by our poor knowledge of the most superficial layers, that might play a prominent part in the response for frequencies larger than 15 Hz. Similar remarks can be made in the case of Station 5. One must note that the two-dimensional model is still too simple because each layer is defined with given wave velocity, density, ... while, as shown in Figs. 11 and 12, our prospection experiments indicate some lateral variations of the elastic modulus in the layer in addition to the variations of depth of the interfaces.

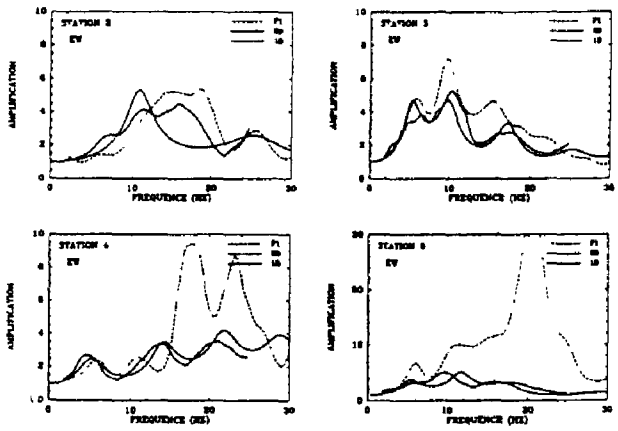

FIGURE 22. Comparison between observed amplification for Group 1, 1D and 2D modeling.

Even if the entire valley is not subject to resonance. 2 D effects cannot be ruled out, in particular to explain local effects at the edges of the structure (Station 2).

In order to point out the influence of the incidence angle $\alpha$ and of Q values, two other computations have been carrried out. The results are presented in Fig.23 which compares the amplifications in the three following cases : (a) $\alpha = 0°$, $Q_S$ = 10, 10, 20, 200 - (b) $\alpha = 30$ , $Q_S$ = 10, 10, 20, 200 - (c) $\alpha = 0^0$, $Q_S$ = 6, 6, 6, 50. The last set of $Q_S$ values correspond to the data inferred from rise time measurements at higher frequencies. The comparison between Figs. 22 and 23 shows that these Q values lead to amplifications much lower than the experimental spectral ratios. The Qs values derived from surface wave analysis in a frequency range close to the sollicitation's one are far more consistent with the observed response.

The other aspect to note in 2D-SH modeling is the influence of the incidence angle on some of the fluctuations of the amplification curves for the different groups of events. This is illustrated in Fig. 23 which compares the amplifications corresponding to angles of incidence of 0 and 30° . One can notice changes in the positions of the amplification peaks as a function of the incidence angle.

In addition, further examination of the whole of the data indicates that a 2D-SH modeling is not sufficient. For example, the different behavior between the two horizontal components (not presented in this paper) is an important point that cannot be addressed at this stage of the simulation. The full elastic modeling and the 3D case must be the next goals of our study.

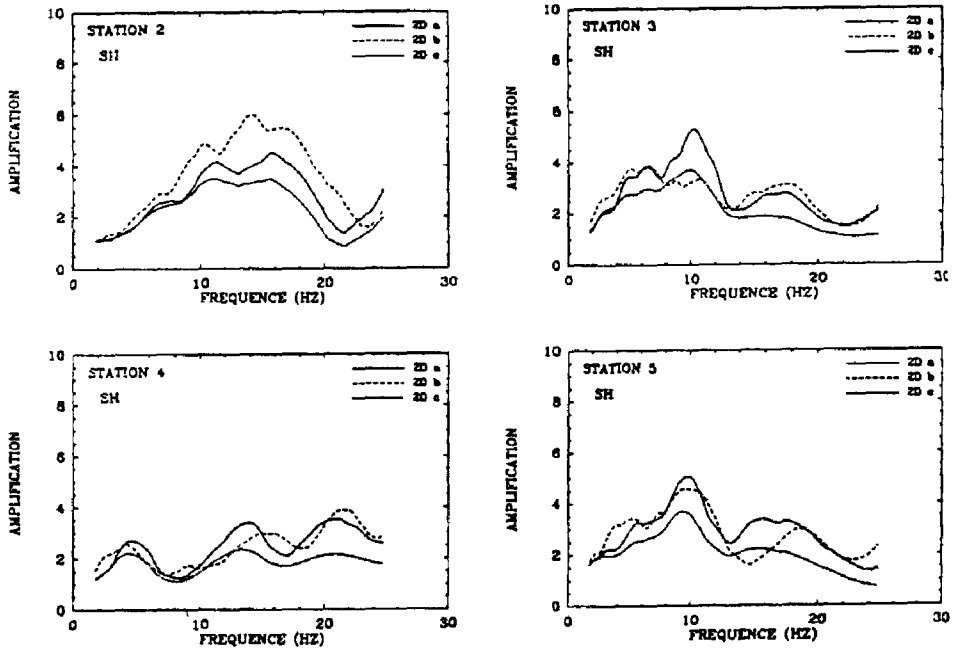


FIGURE 23. Influence of the incidence angle and Q values on the amplification curves See explanations in the text.

## CONCLUSIONS

The study of the Ubaye valley has been initiated with the aim to test our capability to predict amplification effects for a given site.

The geological structure of the valley was unknown and the first step was to investigate it thoroughly with different seismic methods (refraction tests, reflection profile and surface wave inversion). P and S wave velocities as well as quality factor values were inferred from these experiments.

At the same time, earthquakes have been recorded by five stations (3 components) located in the valley and on a rock outcrop. The spectral ratio have pointed out a great variability of the response between the different stations and for different groups of earthquakes at the same station. This last observation suggests an azimuthal dependence of the site response towards the earthquake location.

On the basis of geophysical data, numerical simulations (1D and 2D modeling) were performed for the SH case. Observed and synthetic spectral ratios generally show a good agreement for a

frequency lower than 10 Hz. The Q values used in the computations are those derived from surface wave analysis, in a frequency range close to the sollicitation's one.

Although these results are promising, modeling at this stage was limited to a specific input motion (incident SH waves) and reality clearly appears to be more complex. An important point to stress is that all the experimental amplifications which have not been simulated tend to be higher than those predicted in the SH case.

## REFERENCES


1. Aki K., 1988, Local site effects on strong ground motion. "Earthquake Engineering and Soil dynamics II - Recent advances in ground motion evaluation", June 27-30, Park City, Utah, USA.

2. Herrmann R., 1987, Computer Programs in Seismology, Saint-Louis University, Missouri, U.S.A.

3. Jongmans D., 1990, L'influence des structures géologiques sur l'amplification des ondes sismiques, Ph.D.Thesis, Liege University, Belgium, 280 p.

4. Johnston and Toksöz, 1981, Seismic wave attenuation, S.E.G. Geophysics reprint series N2.

5. Meissner R. and Theilen F., 1986, Experimental studies of the absorption of seismic waves, D.G.M.K.-project 254, pp.5-53.

6. Gladwin M. and Stacey F., 1974, Anelastic degradation of acoustic pulses in rock, Phys.Earth Planet. Int., 8, 332-336.

7. Blair D.P. and Spathis A.T., Seismic source influence in pulse attenuation studies, Journal of Geophysical Research, 89, pp.9253-9258.

8. Jongmans D., 1991, Near source pulse propagation : application to Q determination, submitted to Geophysical Prospecting.

9. Herrmann R.and Mitchell B., 1975, Statistical analysis and Interpretation of surface-wave anelastic attenuation data for the stable interior of North America, Bull.Seism.Soc.Am., 65, pp.1115-1128.

10. Bouchon M, Campillo M. and Gaffet S., 1989, A boundary integral equation-discrete wavenumber representation method to study wave propagation in multilayered media having irregular interfaces, Geophysics, 54, 1134-1140.